Spin-Current Generation in Low-Damping $Ni_{0.65}Zn_{0.35}Al_{0.8}Fe_{1.2}O_4$ Spinel Ferrite

M. T. Gray, S. Emori, B. A. Gray, H. Jeon, O. M. J. van 't Erve, B. T. Jonker, S. Kim, M. Suzuki, T. Ono, B. M. Howe, and Y. Suzuki

Phys. Rev. Applied **9**, 064039 — Published 25 June 2018

DOI: 10.1103/PhysRevApplied.9.064039

Spin Current Generation in a New Low-Damping Spinel Ferrite

M. T. Gray[1,2,a)], S. Emori[2,3], B. A. Gray[4], H. Jeon[4,5], O. M. J. van 't Erve[6], B. T. Jonker[6], S. Kim[7], M. Suzuki[8], T. Ono[7], B. M. Howe[4], and Y. Suzuki[2,9]

1. Department of Materials Science and Engineering, Stanford University, Stanford CA

2. Geballe Laboratory for Advanced Materials, Stanford University, Stanford, CA

3. Department of Physics, Virginia Tech, Blacksburg, VA

4. Materials and Manufacturing Directorate, Air Force Research Laboratory, Dayton, OH

5. Department of Electrical Engineering, Wright State University, Dayton, OH

6. Materials Science and Technology Division, Naval Research Laboratory, Washington, DC

7. Institute for Chemical Research, Kyoto University, Gokasho, Uji, Kyoto, 611-0011, Japan

8. Japan Synchrotron Radiation Research Institute, 1-1-1 Kouto, Sayo, Hyogo 679-5198, Japan

9. Department of Applied Physics, Stanford University, Stanford CA

\- - - - - - - - - - - - -

Low-damping spin sources are critical to efficient spin current generation, but low-damping magnetic insulators have not been systematically explored so that the controlling parameters for efficient spin current generation are not well understood. The choice of magnetic insulators with sufficiently low damping has been largely limited to $Y_3Fe_5O_{12}$ (YIG), whose compatibility with existing microelectronics is problematic at best. Therefore, the discovery of a new material or a new family of magnetic insulators with low damping would provide not only fundamental insight into the underlying mechanisms for low-damping magnetic insulators but also the foundation for a spin current based electronics future. The family of spinel ferrites includes a wide variety of magnetic insulators, but high damping in conventional spinel ferrites has made them poor spin current sources. In this study, we demonstrate that microwave excitation of low-damping (Ni,Zn,Al)-ferrite (NZAFO) efficiently generates spin current. Spin pumping from the ferrite to an adjacent metal layer is manifest in both an increase in Gilbert damping and the emergence of a voltage peak that occurs at ferromagnetic resonance (FMR). Magnetotransport measurements suggest negligible contributions from a proximity-induced magnetic layer in the metal. From FMR and magnetotransport measurements, we estimate the spin-mixing conductance at the NZAFO/Pt interface to be ~10^{14} $\Omega^{-1}m^{-2}$, on the same order of magnitude as the oft-studied YIG/Pt interface. These results indicate that doped spinel ferrites can be efficient spin-pumping sources with potential for highly tunable magnetic properties and coherent integration with a diverse range of complex oxides for all oxide spintronics.

\- - - - - - - - - - - - -

I. INTRODUCTION

Generation, propagation, and detection of spin current have been of fundamental and technological interest due to their myriad applications from information storage to quantum computing [1,2]. Since the demonstration of the spin Hall effect [3,4], many studies have focused on the generation and detection of "pure" spin current with no net charge current in order to reduce power dissipation. One of the most promising approaches to pure spin current generation is spin pumping in thin-film ferro(ferri)magnet (FM)/normal metal (NM) bilayers, where a microwave field excites ferromagnetic resonance (FMR) in the FM layer which leads to a non-equilibrium spin potential (accumulation) at the FM/NM interface [5,6]. This accumulation of spins results in a pure spin current in the NM layer through diffusion, which can then either propagate or be detected depending on the strength of the spin-orbit interaction in the NM.

Insulating magnetic materials are thought to be ideal sources of resonantly excited spin current because of the absence of dissipation by conduction electron scattering [7,8]. These magnetic insulators also do not exhibit electric current shunting that can complicate spin transport analysis in heterostructures based on magnetic conductors. So far, epitaxial iron garnets, particularly $Y_3Fe_5O_{12}$ (YIG), have been the only thin-film magnetic insulators with low enough damping for efficient excitation of spin current [9–15]. However, there are significant disadvantages to YIG: the low effective magnetization leads to high external field requirements (e.g. 0.1 T at 5 GHz, with external field in-plane, and with magnetization in-plane) for ferromagnetic resonance (FMR); the garnet family of materials has limited electronic functionality for isostructural integration; and the complexity of the garnet crystal structure poses an obstacle to coherent integration with other families of crystalline materials [16,17]. As spin pumping in heterostructures requires the transfer of spin information across an interface, the role of interface quality must be understood thoroughly yet remains unclear. Therefore, in order to realize and implement new, highly efficient spin current based electronics, we must identify new materials systems for spin pumping.

Spinel ferrites constitute an alternative class of magnetic materials with a variety of electronic states (insulators, metals, superconductors, multiferroics, etc) and a crystal structure that can be coherently integrated with perovskite materials for an even wider range of functionality [18–20]. Moreover, as evidenced by extensive applications of bulk spinel ferrites in high-frequency electronic components, the magnetic properties of spinel ferrites can be tuned robustly by chemical substitution [21]. However, spinel ferrite thin films have exhibited extremely high damping that makes these materials unsuitable for spin current generation. The only current report of spin pumping using a spinel ferrite as the FM layer [22] is in bilayers of semiconducting Fe_3O_4 interfaced with Pt, which exhibit high loss magnetization dynamics with FMR linewidths ~50 mT and spin pumping signals that are two orders of magnitude smaller than YIG/Pt measured in the same setup [23].

In this study, we demonstrate efficient spin pumping in a low-damping epitaxial spinel thin film system of (Ni,Zn,Al)-ferrite (NZAFO) as the spin-current source. This model system represents a recently developed paradigm for low-damping magnetic insulators with giant easy-plane anisotropy that significantly reduces the external field necessary for FMR at a given frequency [24]. We demonstrate significant spin pumping from the spinel ferrite into an adjacent Pt layer through Gilbert damping enhancement and electrical voltage peaks that appear at FMR. The reversal of the measured voltage signal between NZAFO/Pt and NZAFO/W samples, consistent with the opposite signs of the respective spin Hall angles, indicates that the signal is indeed dominated by the inverse spin Hall effect and not by proximity-induced anisotropic magnetoresistance (AMR). Angular dependent magnetoresistance (ADMR) measurements on NZAFO/Pt reveal the spin Hall magnetoresistance (SHMR) to be ~20 times greater than the proximity-induced AMR, further confirming the dominance of spin current transport over proximity-induced magnetization at the NZAFO/Pt interface. From FMR and ADMR results, we estimate the spin-mixing conductance of the NZAFO/Pt interface to be ~10^{14} $\Omega^{-1}m^{-2}$. Thus, we have shown the viability of using doped spinel ferrites, such as NZAFO, for efficient spin-pumping, opening up opportunities for broader materials integration and device development.

II. METHODS

$Ni_{0.65}Zn_{0.35}Al_{0.8}Fe_{1.2}O_4$ (NZAFO) films (15 nm thick) were grown on (001) oriented, single crystalline 5×5 mm^2 $MgAl_2O_4$ (MAO) substrates using pulsed laser deposition (PLD). A KrF laser operating at 4 Hz with a fluence of 4 J/cm^2 ablated a polycrystalline target of $Ni_{0.65}Zn_{0.35}Al_{0.8}Fe_{1.2}O_4$ in order to grow thin films of NZAFO. The substrate was held at 550°C in an atmosphere of 300 mTorr O_2 during deposition and cooling. Pt films (1.5 or 2.5 nm thick) were subsequently deposited in-situ with PLD at 1 Hz, 25°C, 10^{-7} Torr (chamber base pressure), and 1.4 J/cm^2 on some NZAFO samples while the rest remained as bare NZAFO films. A PANalytical X'Pert X-ray Diffractometer was used to measure symmetric θ–2θ scans, ω rocking curves, low-angle reflectivity, and reciprocal space maps in order to confirm the epitaxial growth, crystalline quality, thickness, and strain state of the NZAFO. Static magnetic characterization was undertaken using a Quantum Design SQUID magnetometer. FMR and the ISHE were measured in a coplanar waveguide based setup with the static field applied in the plane of the samples along the (100) direction. Broadband FMR spectra were acquired using a coplanar waveguide with a central conductor width of 250 µm and microwave diode combined with field modulation (see [24] for more information), while spin pumping voltage spectra were acquired using a nanovoltmeter measuring transverse to the static magnetic field. The nominal microwave power for all these measurements was set to 23 dBm. For magnetotransport measurements, NZAFO/Pt bilayers were patterned by Ar ion milling into 500-µm wide Hall bars with longitudinal contacts separated by 2 mm and a contact width for the voltage contacts of 0.1 mm. Magnetotransport results were obtained from these Hall bar samples at 300 K in a Quantum Design Dynacool system.

III. RESULTS

A. Structure

We have developed highly crystalline, fully strained $Ni_{0.65}Zn_{0.35}Al_{0.8}Fe_{1.2}O_4$ (NZAFO) thins films. The very low defect density in these films is critical to the observed low damping behavior and distinguishes them from typical spinel ferrite thin films [25,26]. X-ray diffraction indicates high quality growth of NZAFO on (001) oriented $MgAl_2O_4$ (MAO) substrates (a = 8.083 Å) with evidence for only the (00*l*) family of peaks in the symmetric θ–2θ scan, strong Laue oscillations indicating smooth interfaces, and a full width at half maximum rocking curve linewidth $\omega < 0.03°$ (figure 1a,b). By substituting a large fraction of Fe^{3+} with smaller Al^{3+}, the $Ni_{0.65}Zn_{0.35}Fe_2O_4$ lattice parameter (a = 8.37 Å) has been greatly reduced allowing fully coherent epitaxial growth of this spinel ferrite material on MAO with an out-of-plane strain of 2.5% as observed by reciprocal space mapping [24]. This coherent epitaxial strain leads to unusually large easy-plane magnetic anisotropy, which is beneficial for attaining FMR with a low bias magnetic field. More importantly, the coherent epitaxy eliminates misfit dislocations, which are sources of defect-mediated damping that is typically present in conventional spinel ferrite films [25,26]. We also note that the NZAFO film surface is very smooth, with typical roughness deduced by atomic force microscopy and X-ray reflectivity of 1-2 Å, much smaller than the spinel lattice parameter. The smooth surface permits a sharp interface between NZAFO and Pt. The high quality interface and low defect density allow for efficient spin pumping in NZAFO/Pt systems.

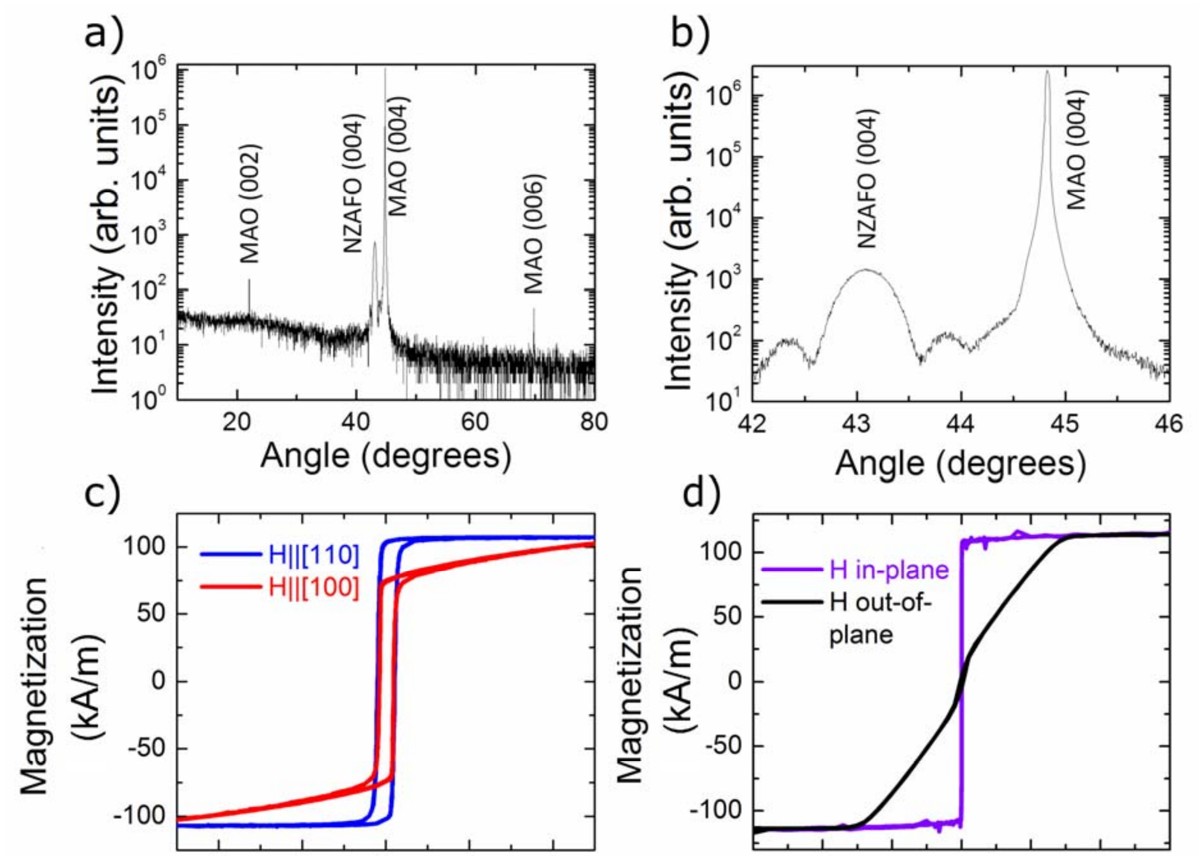

Figure 1 – Structural and static magnetic characterization of NZAFO. a) Symmetric θ-2θ XRD scan showing no evidence of secondary phases or orientations. b) Zooming in on the NZAFO (004) peak shows the Laue oscillations indicative of smooth NZAFO interfaces. c) In-plane SQUID measurements

showing the low coercive field and anisotropy field. d) Comparison of in-plane and out-of-plane SQUID demonstrating the large easy-plane magnetic anisotropy field.

B. Static Magnetism

Bulk SQUID magnetometry confirms that epitaxial NZAFO exhibits a remarkable combination of very soft in-plane magnetism and giant negative perpendicular uniaxial anisotropy. NZAFO shows a small amount of cubic in-plane anisotropy with the in-plane <110> directions being the easy axes (figure 1c). For all in-plane directions the coercive field is extremely small - less than 0.2 mT. We attribute the soft magnetic anisotropy to Zn and Al doping and to the minimization of defects due to lattice matching of the NZAFO film with the commercially available MAO substrates [24]. The out-of-plane direction is magnetically hard, with an anisotropy field greater than 1 T and significantly larger than the expected shape anisotropy of <0.2 T (figure 1d). This very large easy-plane anisotropy (negative perpendicular magnetic anisotropy) is driven by a combination of strong magnetostriction and large epitaxial strain which leads to significant tetragonal distortion in the film [24]. The combination of giant easy-plane anisotropy and soft in-plane magnetism provides for low damping and reduces the magnitude of external field required to attain FMR.

C. Ferromagnetic Resonance and Spin Pumping

The low defect density and soft in-plane magnetism of NZAFO thin films allow for reliable measurements of FMR over a wide range of excitation frequencies, permitting investigation of the static and dynamic magnetic properties of NZAFO thin films and NZAFO/Pt interfaces. The absorption of the films at the resonance condition exhibits a clean, Lorentzian derivative from which the FMR field H_{FMR} and half-width-at-half-maximum FMR linewidth ΔH are extracted. The frequency dependence of the FMR field allows for the quantification of magnetic anisotropy, and we see that the addition of Pt does not significantly alter the static magnetic properties. The frequency dependence of the FMR linewidth is then used to quantify the Gilbert damping in NZAFO; the enhancement in Gilbert damping with the addition of a Pt overlayer allows estimation of the spin-mixing conductance at the interface. Finally the opposite voltage generated at FMR in NZAFO/Pt and NZAFO/W confirms the presence of strong spin-pumping at these interfaces.

Complementary to the SQUID magnetometry results, we can quantify static magnetic properties through fitting of the frequency dependence of FMR to the Kittel equation

$$f = \frac{g\mu_B}{h}\mu_0\sqrt{\left[H_{FMR} + H_{cub}\cos 4\phi\right]\left[H_{FMR} + H_{cub}\left(\frac{3+\cos 4\phi}{4}\right) + M_{eff}\right]} \quad \text{(eqn 1)}$$

where h is Plank's constant, g is the Landé g factor, μ_0 is the permeability of free space, μ_B is the Bohr magneton, ϕ is the in-plane angle between H and the [100] direction, H_{cub} is the in-plane cubic magnetocrystalline anisotropy field, and $M_{eff} = M_s - H_u$ is the effective magnetization that includes the contributions from the saturation magnetization (out-of-plane demagnetizing field) M_s and the out-of-plane uniaxial magnetoelastic anisotropy field H_u. A negative value of H_u indicates that the film has a magnetic anisotropy composed of an easy plane and hard perpendicular axis. We fit the frequency dependence (figure 2a) of the resonance field, H_{FMR}, measured with the in-plane external magnetic field applied along [100] (ϕ=0). From the fit shown in figure 2a, we find g = 2.32±0.03, $\mu_0 H_{cub}$ = -6.0±0.1 mT, and $\mu_0 M_{eff}$ = 1.15±0.03 T, in good agreement with prior work [24].

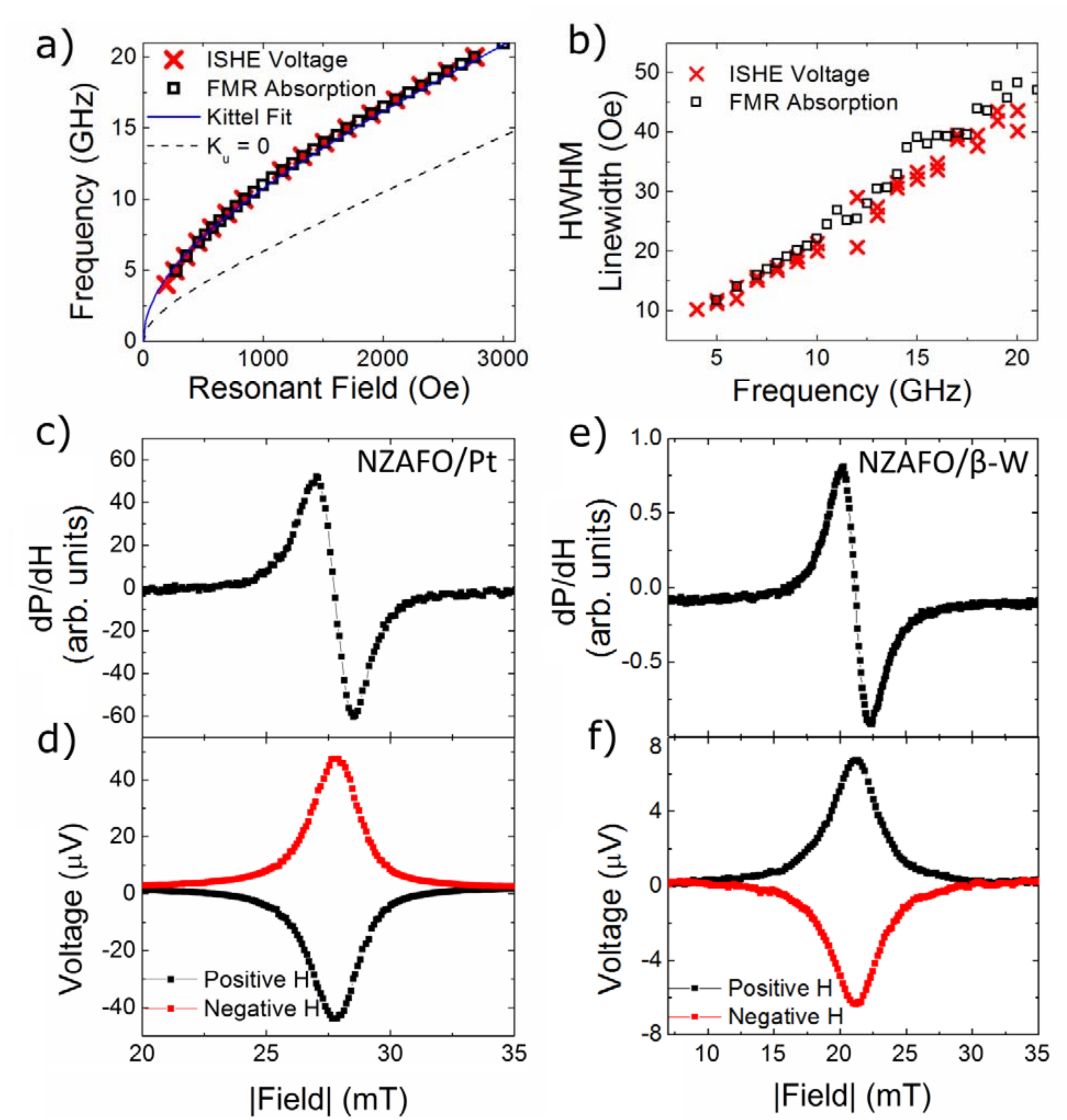

Figure 2 – a) FMR resonance field vs frequency derived from the microwave absorption results and the FMR driven voltage. The dashed line shows the Kittel fit in the absence of the K_u term, the perpendicular magnetic anisotropy, directly demonstrating the significant suppression of the external field requirements. b) FMR Linewidth vs frequency. The excellent correspondence in both resonance frequency vs external field and frequency vs linewidth confirm that the voltage is driven by the FMR and

this voltage measurement can be used to accurately characterize the FMR behavior of NZAFO. c,e) Microwave power absorption derivative and the corresponding voltages (d and f) for NZAFO/Pt, and NZAFO/W at 5 GHz. The opposite sign of the voltage response seen in (d) and (f) is caused by the opposite spin Hall angle in W and Pt and indicates that the observed voltage is dominated by the ISHE and not by AMR.

The value of $\mu_0 M_{eff}$, which is well in excess of the shape anisotropy field $\mu_0 M_s$ = 0.15±0.01 T, confirms the presence of giant strain-induced easy-plane anisotropy (negative perpendicular magnetic anisotropy) with $\mu_0 H_u$ = -1.00±0.04 T, consistent with the large out-of-plane saturation field observed via SQUID magnetometry (figure 1d). The magnitude of the perpendicular uniaxial anisotropy energy density $K_u = \frac{\mu_0 H_u M_s}{2}$ = -60±2.4 kJ/m^3 is also two orders of magnitude greater than the in-plane cubic anisotropy energy density $K_{4||} = \frac{\mu_0 H_{cub} M_s}{2}$ = -0.4±0.02 kJ/m^3, further corroborating the dominance of the strain-induced anisotropy. This strong negative K_u term leads to a suppression of the resonance field for a given frequency which saves both space and energy in device applications. The suppression can be seen directly through the K_u = 0 line in figure 2a, which is derived from the same Kittel fit parameters in the absence of the K_u term. For example, at 5 GHz the external field requirement is four times lower than it would be without the negative perpendicular uniaxial anisotropy and is also four times lower than YIG at the same frequency. The strength of this term is driven by the large amount of coherent epitaxial strain and strong magnetoelastic coupling present in NZAFO [24]. This magnetoelastic coupling is also reflected in the deviation of the Landé g-factor (g≈2.3) from the spin-only value of 2.0, indicating a substantial orbital contribution to magnetism that is essential for coupling lattice strain to magnetism [24].

We are unable to detect any systematic change in “static” magnetic properties due to the addition of a Pt interface. Both the magnetic anisotropy and Landé g-factor do not change systematically with the addition of Pt. This is in contrast with a prior study showing systematic shifts of the FMR field in YIG with the addition of Pt, which has been interpreted to be an indication of static magnetic coupling (Pt proximity-induced magnetization) across the YIG/Pt interface [11].

The effect of an adjacent spin-orbit metal on the linewidth of the absorption peaks gives insight into the spin-pumping driven damping present in the system. As shown in figure 3 the FMR linewidth is significantly increased by the presence of a 2.5 nm Pt layer for all measured frequencies. This increase in damping is attributed to spin current from the NZAFO layer to the conduction electrons in the adjacent Pt layer. Damping in FMR is typically modeled in terms of the Gilbert damping parameter α [5,6], which is extracted from the linear fit of the linewidth against frequency,

$$\Delta H = \Delta H_0 + \frac{2\pi}{|\gamma|\mu_0}\alpha f \quad \text{(eqn 2)}$$

where ΔH_0 is the extrapolated zero frequency linewidth and $|\gamma| = g\mu_B / \hbar$ is the gyromagnetic ratio [27,28]. NZAFO and NZAFO/Pt films exhibit linewidths that scale linearly up to the instrumental limit, allowing for a reliable, empirical extraction of α.

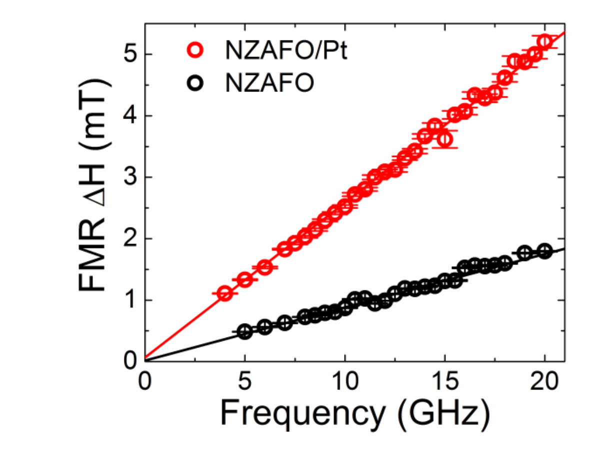

Figure 3 – FMR microwave absorption linewidth vs frequency for NZAFO and NZAFO/Pt thin films. The addition of a 2.5 nm Pt layer significantly increases the damping due to spin scattering and spin-mixing at the ferromagnet/heavy metal interface. By fitting this relation to equation 2, we can extract a Gilbert damping parameter of ~0.003 for the bare NZAFO films and ~0.007 for the films capped with Pt.

We see an increase in the Gilbert damping parameter from ~0.003 to ~0.007 upon the addition of 2.5 nm thick Pt. Such an increase in damping can be used to quantify the strength of the spin pumping, parameterized by an "effective" spin-mixing conductance, G_{eff},

$$\alpha = \alpha_0 + \frac{|\gamma|\hbar^2}{2e^2 M_S t_{FM}} G_{eff} \quad \text{(eqn 3)}$$

where ħ is the reduced Plank constant, e is the electron charge, and t_{FM} is the NZAFO layer thickness [29]. We obtain $G_{eff} \approx 1.2\times10^{14}\ \Omega^{-1}m^{-2}$ for our NZAFO/Pt interfaces, comparable to YIG/Pt interface values in the range $G_{\uparrow\downarrow} \approx (0.6\text{-}4)\times10^{14}$ [11,13,30–32]. G_{eff} can be decomposed into the interfacial spin-mixing conductance and the bulk spin conductance governed by the resistivity ρ_{Pt}, spin diffusion length λ_s, and thickness t_{Pt} of Pt [6,29]:

$$G_{eff} = \left[\frac{1}{G_{\uparrow\downarrow}} + 2\rho_{Pt}\lambda_s \coth\left(\frac{t_{Pt}}{\lambda_s}\right) \right]^{-1} \quad \text{(eqn 4)}$$

With $\rho_{Pt} = 5.0\times10^{-7}\ \Omega m$ obtained from a 4-point resistance measurement and $\lambda_s \approx 1.5$ nm based on Nguyen et al. [33], we derive $G_{\uparrow\downarrow} \approx 4\times10^{14}\ \Omega^{-1}m^{-2}$. We note, however, that here we have ignored interfacial spin scattering (due to "spin memory loss" or disorder effects) which may give rise to enhanced damping in this system [34–37]. Thus, the enhanced damping alone does not definitively indicate spin pumping across the NZAFO/Pt interface.

D. Electrical Detection of Spin Pumping

As an alternative means to detect spin pumping, the microwave response of NZAFO/Pt bilayers was measured electrically to detect an inverse spin Hall effect in 1.5 nm thick Pt films. The transmission of resonantly excited spin current from a magnetic layer to a nonmagnetic metal can be detected through the dc voltage generated across the metal by the conversion of spin current into a charge accumulation due to the inverse spin Hall effect. We observe a peak in the voltage signal as a function of magnetic field (e.g. figure 2d at 5 GHz) at the same field as the microwave absorption peak (e.g. figure 2c at 5 GHz). The frequency dependence of the voltage peak linewidth and resonance field are in excellent agreement with the microwave absorption results as seen in figure 2a,b. We note that in this coplanar waveguide setup, an accurate quantitative analysis of spin pumping efficiency (i.e., spin Hall angle) is difficult due to the lack of a precise calibration of microwave magnetic field. Nevertheless, the voltage peak amplitude on the order of 10 μV in NZAFO/Pt is comparable to previously reported spin pumping signal amplitudes in YIG/Pt with the microwave excitation generated by a coplanar waveguide [13,31,32].

Despite being linked to the FMR response, the voltage signal may be explained by mechanisms other than spin pumping. For example, large voltage peaks at FMR are known to arise from "spin rectification," the mixing of oscillating magnetoresistance and induced microwave currents in magnetic *conductors* [38–40]. Since Pt is quite close to a ferromagnetic transition according to the Stoner criterion, it is susceptible to proximity-induced magnetism: at interfaces with a magnetic insulator Pt can develop long range magnetic order coupled to the magnetization of the FM layer, such as YIG [11,41,42]. It is also possible that an off-stoichiometry at the NZAFO surface makes the ferrite weakly conductive. Such an interfacial conductive magnetic layer – whether it is in the Pt or ferrite – could exhibit non-negligible anisotropic magnetoresistance, which may potentially give rise to a resonant spin rectification voltage similar to FM/NM bilayers.

In order to demonstrate that the observed voltage is dominated by the Inverse Spin Hall Effect (ISHE), we also measured $Ni_{0.65}Zn_{0.35}AlFeO_4$/W interfaces (sample details given in Supplementary Note 1 [43]). Although linewidths of these $Ni_{0.65}Zn_{0.35}AlFeO_4$ films are about twice as high as that of the $Ni_{0.65}Zn_{0.35}Al_{0.8}Fe_{1.2}O_4$ films in the NZAFO/Pt batch, the static magnetic properties (M_s, coercive field, anisotropy, etc.) are very similar to the $Ni_{0.65}Zn_{0.35}Al_{0.8}Fe_{1.2}O_4$ in the NZAFO/Pt batch. The β phase of W is well known to have a spin Hall angle of opposite sign compared to that of Pt [30,44,45]. NZAFO/W interfaces show a voltage response that also tracks well with the FMR microwave absorption and is opposite in sign to the NZAFO/Pt interfaces (e.g. figure 2e,f at 5 GHz). If the voltage signals are attributed to rectified anisotropic magnetoresistance in the metal layer due to proximity-induced ferromagnetic coupling across the interface, the voltage signal should have the same sign in both systems (see Supplementary Note 1 for further discussion [43,46–48]). The inverse Rashba-Edelstein effect (IREE) at the NZAFO/metal interface is another proposed mechanism that generates a voltage peak from spin pumping [49], since the IREE has the same symmetry as ISHE. However, at this point, while it is theoretically well established that the spin Hall angles in the bulk of Pt and W have opposite sign [44], it is less clear that the signs of the Rashba coefficient should be opposite for NZAFO/Pt and

NZAFO/W. Therefore, we attribute the observed sign difference between the two systems to spin-pumping across the NZAFO/NM interface and the ISHE in the NM.

E. Magnetotransport

Magnetoresistance (MR) measurements can also provide insight into the spin transport across the NZAFO/NM interface, complementary to the FMR-based experiments described above. In particular, the angular dependent magnetoresistance (ADMR) permits us to quantify the relative magnitudes of interfacial spin transport and proximity-induced magnetism, as well as independently estimate the spin-mixing conductance. Spin Hall magnetoresistance (SHMR) occurs in thin metallic layers with strong spin-orbit coupling when interfaced with ferro(ferri)magnets and has been observed in a number of systems [50–54]. SHMR relies on the ISHE and a similar transfer of angular momentum across the interface as in the FMR-driven spin-pumping and therefore has a strong angular dependence. However, there are other possible contributions to the magnetoresistance such as AMR and Hanle MR [55,56] which have different dependencies on the magnetic field strength and orientation. In order to separate out these different contributions, we performed a series of MR measurements in different current and field configurations.

The angular dependence of the magnetoresistance (ADMR) allows for independent quantification of the relative strength of SHMR and AMR at this interface. Critically AMR depends on the component of M along the j direction (see figure 4a-c for directional definitions) while SHMR depends on the component of M along the t direction. More specifically, the contributions to the longitudinal ADMR expected for these two phenomena are given by

(AMR) $\rho = \rho_0 + \Delta\rho_{AMR} m_j^2$ (eqn 5)

(SHMR) $\rho = \rho_0 + \Delta\rho_{SHMR} m_t^2$ (eqn 6)

where $m_j = \frac{M \bullet \hat{j}}{|M|}$; $m_t = \frac{M \bullet \hat{t}}{|M|}$; $\rho = \frac{Vwt_{Pt}}{LI}$; M is the magnetization, V is the longitudinal voltage, I is the current, and w and L are the Pt dimensions [53].

Although AMR and SHMR exhibit identical angular dependence when the magnetization is rotated in the film plane, SHMR and AMR can be disentangled by rotating the magnetization from in-plane to out-of-plane [52,53] as illustrated in figure 4a,b. Given the strong out-of-plane magnetic anisotropy of NZAFO thin films, the orientation of the magnetization at a given external field must also be taken into account. We can calculate this M orientation by assuming the magnetization rotates as a single domain and minimizing the free energy given by [53,57,58]

$$F = -\mu_0 H \bullet M + \frac{1}{2}\mu_0 M_S \left[M_{eff} \cos^2\theta_M - \frac{1}{8} H_{cub} \left(3 + \cos 4\phi\right) \sin^4\theta_M \right] \text{ (eqn 7)}$$

where ▯$_M$ is the angular displacement from the n direction. The values for M_{eff} and H_{cub} in equation 7 are determined from FMR absorption measurements and supported by the static magnetometry results. Note that due to the large negative perpendicular anisotropy, even at 2 T there is significant misalignment in the out-of-plane rotations. This misalignment can be seen in figure 4d,e where deviation from the simple cosine squared dependence is observed, but accounting for the correct M orientation allows for excellent matching between theory and experiment. Comparing figure 4d,e with equations 5 and 6, we also note that the resistivity in figure 4d is higher when the applied field is in the j direction than the n direction, thus making $\Delta\rho_{AMR}$ positive. In figure 4e the resistivity is higher when the field is in the n direction than the t direction, thus making $\Delta\rho_{SHMR}$ negative. Since the ADMR in the γ rotation is dominated by ρ_{SHMR}, as will be discussed shortly, we plot figure 4f in a similar fashion to 4e. Therefore, the opposite signs of AMR and SHMR follow from the definitions given in equations 5 and 6.

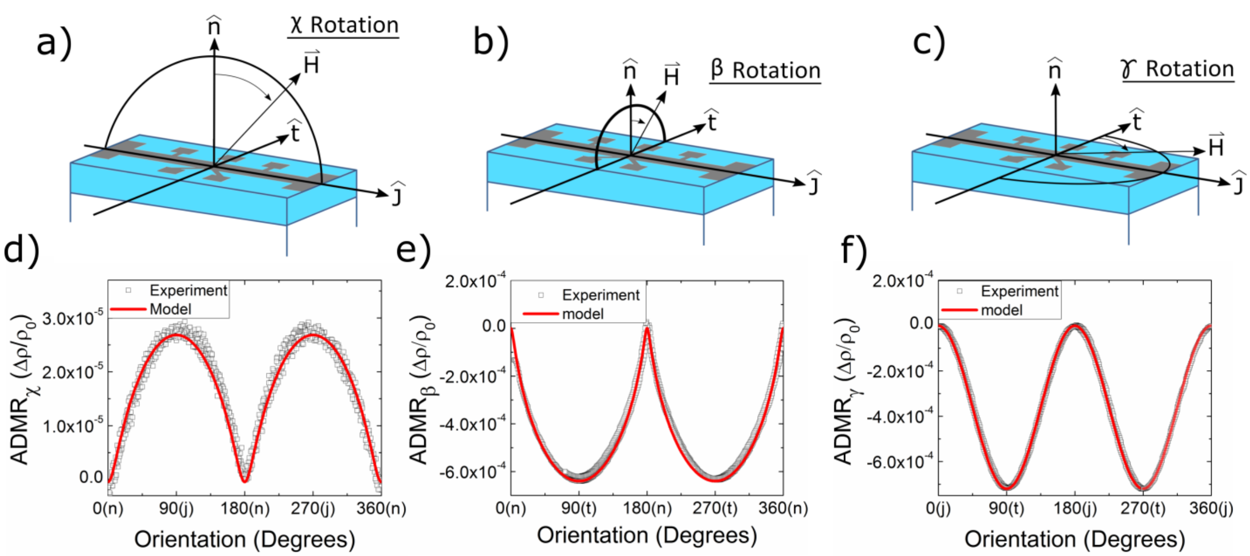

Figure 4 – a-c) Schematics of the patterned NZAFO/Pt sample with directional definitions. χ rotations correspond to rotating H in the $\hat{j}\hat{n}$ plane (a), β in the $\hat{t}\hat{n}$ plane (b), and γ in the $\hat{t}\hat{j}$ plane (c). d-f) Measured and modeled longitudinal ADMR of 2.5 nm Pt films on NZAFO at 300 K and 2 T in the χ, β, and γ rotations, respectively. Note the much smaller ADMR strength for the χ rotation data. Explicitly, the y-axes in 4d-f ($\Delta\rho/\rho_0$) are defined as $\frac{(\rho-\rho_n)}{\rho_n}$ for 4d, $\frac{(\rho-\rho_n)}{\rho_n}$ for 4e, and $\frac{(\rho-\rho_j)}{\rho_j}$ for 4f where ρ_n and ρ_j are the resistivities when the field is applied along the n and j directions respectively. At this field the misalignment between M and H due to the perpendicular magnetic anisotropy can be clearly seen. In order to model the ADMR we use either AMR or SHMR theory (equations 5 and 6) and determine the magnetization angle using a free energy minimization calculation (equation 7).

This fitting procedure allows us to extract ρ_{SHMR} from the β sweep and ρ_{AMR} from the χ sweep (see figure 4a,b). The β sweep results depend strongly on the magnitude of the external field (figure 5), which can be attributed to Hanle magnetoresistance – a phenomenon analogous to SHMR except that it depends on the external magnetic field instead of the adjacent layer's magnetization [55]. This effect should be approximately parabolic in field [56], and the low field intercept gives the SHMR ratio $|\Delta\rho_{SHMR}|/\rho_0 \approx 6\times10^{-4}$, which agrees well with results reported for YIG/Pt interfaces in the range $|\Delta\rho_{SHMR}|/\rho_0 \approx (0.4\text{-}10)\times10^{-4}$ [31,53,54,59,60]. By contrast, the χ sweep exhibits no significant H dependence, which is consistent with the fact that AMR depends on the orientation of M but not H. As seen in figure 4d,e and figure 5 these fits imply that SHMR is ~20 times greater than AMR. From these results, we confirm that spin transport across the NZAFO/Pt interface dominates over contributions from interfacial proximity-induced magnetism. This is in line with our conclusion that the resonant spin pumping voltage is dominated by the ISHE (Section III-D), as well as the lack of detectable Pt magnetism within the resolution limit of X-ray circular dichroism as shown in Supplementary Note 2 [43,61–63].

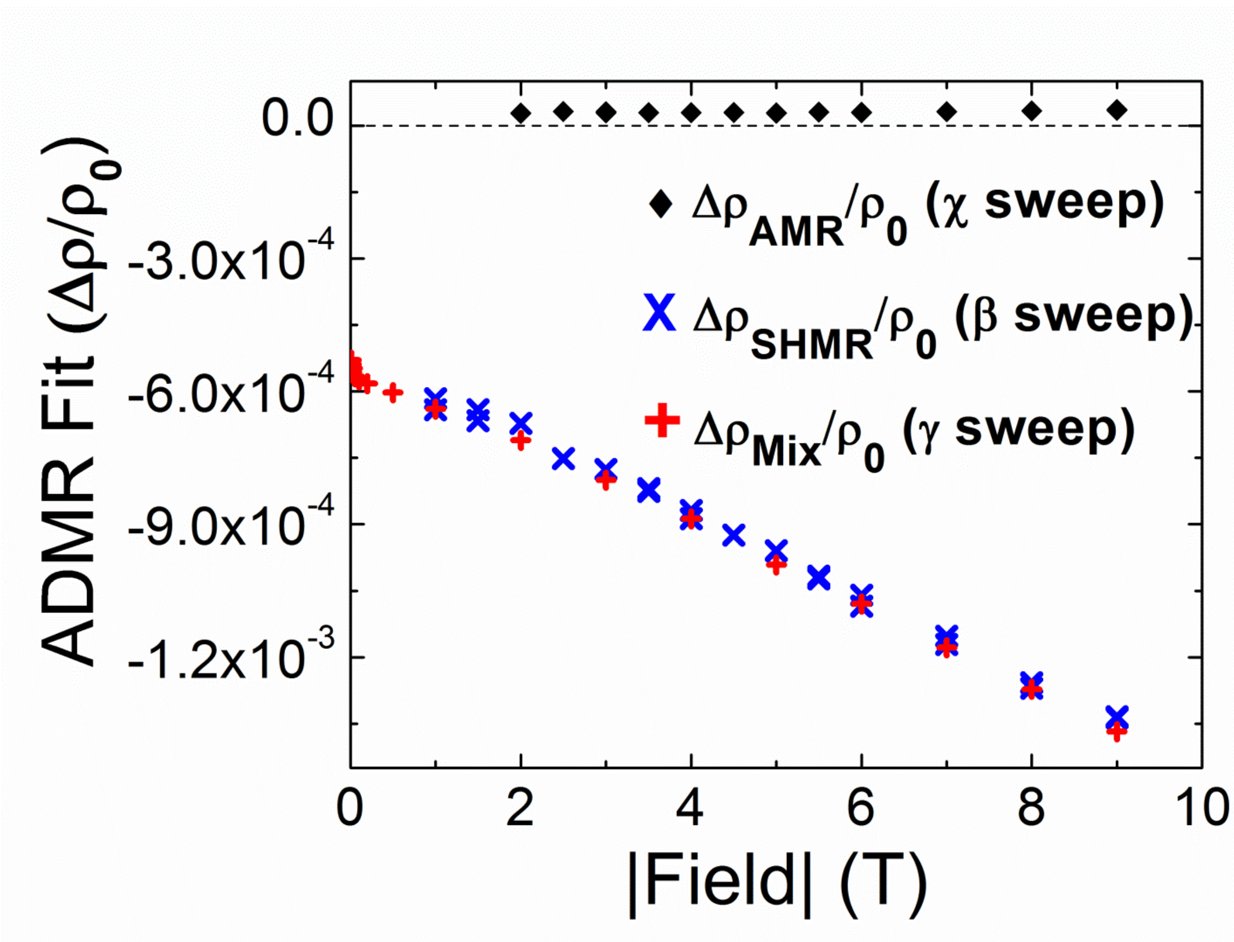

Figure 5 – Field dependence of the coefficients ρ_{SHMR} and ρ_{AMR} derived from ADMR in various orientations (see figure 4a-c) using equations 5 and 6 and following the definitions outlined in the figure 4 caption. The strong, roughly quadratic field dependence of the β and γ sweeps is indicative of Hanle MR. The lack of similar field dependence in the χ sweep indicates that the signal in this orientation is from AMR and not sample misalignment. The reduced anisotropy of the γ sweep allows for lower external field measurements, and thus more accurate extraction of the low field intercept (the SHMR contribution).

Using the $\Delta\rho_{SHMR}$ and ρ_0 values extracted from ADMR, we can obtain an estimate of the spin-mixing conductance from [51,53,54]

$$\frac{-\Delta\rho_{SHMR}}{\rho_0} = \frac{\theta_{SH}^2\left(2\lambda_{Pt}^2\rho_{Pt}\right)\left(t_{Pt}\right)^{-1} G_{\uparrow\downarrow}\tanh^2\left(\frac{t_{Pt}}{2\lambda_{Pt}}\right)}{1+2\lambda_{Pt}\rho_{Pt}G_{\uparrow\downarrow}\coth\left(\frac{t_{Pt}}{\lambda_{Pt}}\right)} \quad \text{(eqn 8)}$$

where θ_{SH} is the spin Hall angle, t_{Pt} = 2.5 nm is the Pt layer thickness, $\rho_{Pt} = 5\times10^{-7}$ Ωm is the resistivity of the Pt layer and λ_{Pt} is the spin diffusion length. Taking the Pt spin diffusion length to be 1.5 nm [53] and the Pt spin Hall angle 0.1 [30,53], we arrive at an interfacial spin-mixing conductance of $G_{\uparrow\downarrow} \sim 10^{14}\ \Omega^{-1}\text{m}^{-2}$, which is on the same order of magnitude as that estimated from FMR damping enhancement.

IV. CONCLUSIONS

We have demonstrated an insulating spinel ferrite compound NZAFO to be an excellent source of resonantly excited spin current which is made possible by the exceptionally low damping of NZAFO. We observe evidence of spin transport across NZAFO/Pt through an enhancement of Gilbert damping as well as voltage peaks that correspond to FMR. The opposite voltage polarities for NZAFO/Pt and NZAFO/W indicate that the signals indeed arise from spin pumping and the ISHE. Complementary angular-dependent magnetoresistance measurements confirm the dominance of interfacial spin transport over signals from very weak proximity-induced magnetism. Our development of a design paradigm for low-damping magnetic insulators based on giant easy-plane anisotropy and demonstration of efficient spin pumping with NZAFO paves the way for high-frequency spintronics that leverage the promising characteristics of spinel ferrites including chemically tunable magnetism, reduced external field requirements, and epitaxial integration with a wide variety of functional complex oxides.

ACKNOWLEDGEMENTS

We thank U. S. Alaan, M. J. Veit, A. El-Ghazaly, N. Sato, R. M. White, and S. X. Wang for insightful discussions on sample growth, Rashba effects, and static & dynamic magnetic characterization. This work was funded by Vannevar Bush Faculty Fellowship program sponsored by the Basic Research Office of the Assistant Secretary of Defense for Research and Engineering and funded by the Office of Naval Research through grant N00014-15-1-0045. In addition, this material is based upon work supported by the Air Force Office of Scientific Research under award number FA9550-15RXCOR198. Part of this work was performed at the Stanford Nano Shared Facilities (SNSF), supported by the National Science Foundation under award ECCS-1542152.

[1] I. Žutić, J. Fabian, and S. Das Sarma, Spintronics: Fundamentals and applications, Rev. Mod. Phys. **76**, 323 (2004).

[2] S. Das Sarma, J. Fabian, X. Hu, and I. Žutić, Spin electronics and spin computation, Solid State Commun. **119**, 207 (2001).

[3] J. E. Hirsch, Spin Hall effect, Phys. Rev. Lett. **83**, 1834 (1999).

[4] E. Saitoh, M. Ueda, H. Miyajima, and G. Tatara, Conversion of spin current into charge current at room temperature: Inverse spin-Hall effect, Appl. Phys. Lett. **88**, 1 (2006).

[5] Y. Tserkovnyak, A. Brataas, and G. E. W. Bauer, Spin pumping and magnetization dynamics in metallic multilayers, Phys. Rev. B **66**, 224403 (2002).

[6] Y. Tserkovnyak, A. Brataas, and G. E. W. Bauer, Enhanced Gilbert Damping in Thin Ferromagnetic Films, Phys. Rev. Lett. **88**, 117601 (2002).

[7] M. A. W. Schoen, D. Thonig, M. L. Schneider, T. J. Silva, H. T. Nembach, O. Eriksson, O. Karis, and J. M. Shaw, Ultra-low magnetic damping of a metallic ferromagnet, Nat. Phys. **12**, 839 (2016).

[8] C. K. A. Mewes and T. Mewes, *Handbook of Nanomagnetism,* (2015).

[9] Z. Qiu, K. Ando, K. Uchida, Y. Kajiwara, R. Takahashi, H. Nakayama, T. An, Y. Fujikawa, and E. Saitoh, Spin mixing conductance at a well-controlled platinum/yttrium iron garnet interface, Appl. Phys. Lett. **103**, 92404 (2013).

[10] H. L. Wang, C. H. Du, Y. Pu, R. Adur, P. C. Hammel, and F. Y. Yang, Large spin pumping from epitaxial $Y_3Fe_5O_{12}$ thin films to Pt and W layers, Phys. Rev. B **88**, 100406 (2013).

[11] Y. Sun, H. Chang, M. Kabatek, Y. Y. Song, Z. Wang, M. Jantz, W. Schneider, M. Wu, E. Montoya, B. Kardasz, B. Heinrich, S. G. E. te Velthuis, H. Schultheiss, and A. Hoffmann, Damping in yttrium iron garnet nanoscale films capped by platinum, Phys. Rev. Lett. **111**, 106601 (2013).

[12] M. C. Onbasli, A. Kehlberger, D. H. Kim, G. Jakob, M. Kläui, A. V. Chumak, B. Hillebrands, and C. A. Ross, Pulsed laser deposition of epitaxial yttrium iron garnet films with low Gilbert damping and bulk-like magnetization, APL Mater. **2**, 106102 (2014).

[13] M. B. Jungfleisch, A. V. Chumak, A. Kehlberger, V. Lauer, D. H. Kim, M. C. Onbasli, C. A. Ross, M. Kläui, and B. Hillebrands, Thickness and power dependence of the spin-pumping effect in $Y_3Fe_5O_{12}$/Pt heterostructures measured by the inverse spin Hall effect, Phys. Rev. B **91**, 134407 (2015).

[14] H. Chang, P. Li, W. Zhang, T. Liu, A. Hoffmann, L. Deng, and M. Wu, Nanometer-Thick Yttrium Iron Garnet Films with Extremely Low Damping, IEEE Magn. Lett. **5**, 6882836 (2014).

[15] O. d'Allivy Kelly, A. Anane, R. Bernard, J. Ben Youssef, C. Hahn, A. H. Molpeceres, C. Carrétéro, E. Jacquet, C. Deranlot, P. Bortolotti, R. Lebourgeois, J. C. Mage, G. De Loubens, O. Klein, V. Cros, and A. Fert, Inverse spin Hall effect in nanometer-thick yttrium iron garnet/Pt system, Appl. Phys. Lett. **103**, 82408 (2013).

[16] F. J. Wong and S. Ramanathan, Nonisostructural complex oxide heteroepitaxy, J. Vac. Sci. Technol. A **32**, 40801 (2014).

[17] A. R. Kaul, O. Y. Gorbenko, and A. A. Kamenev, The role of heteroepitaxy in the development of new thin-film oxide-based functional materials, Russ. Chem. Rev. **73**, 861 (2007).

[18] U. Lüders, A. Barthélémy, M. Bibes, K. Bouzehouane, S. Fusil, E. Jacquet, J. P. Contour, J. F. Bobo, J. Fontcuberta, and A. Fert, $NiFe_2O_4$: A versatile spinel material brings new opportunities for

spintronics, Adv. Mater. **18**, 1733 (2006).

[19] U. Lüders, G. Herranz, M. Bibes, K. Bouzehouane, E. Jacquet, J. P. Contour, S. Fusil, J. F. Bobo, J. Fontcuberta, A. Barthálámy, and A. Fert, Hybrid perovskite-spinel magnetic tunnel junctions based on conductive ferrimagnetic $NiFe_2O_4$, J. Appl. Phys. **99**, 08K301 (2006).

[20] B. B. Nelson-Cheeseman, R. V. Chopdekar, L. M. B. Alldredge, J. S. Bettinger, E. Arenholz, and Y. Suzuki, Probing the role of the barrier layer in magnetic tunnel junction transport, Phys. Rev. B **76**, 220410 (2007).

[21] V. G. Harris, Modern microwave ferrites, IEEE Trans. Magn. **48**, 1075 (2012).

[22] F. D. Czeschka, L. Dreher, M. S. Brandt, M. Weiler, M. Althammer, I. M. Imort, G. Reiss, A. Thomas, W. Schoch, W. Limmer, H. Huebl, R. Gross, and S. T. B. Goennenwein, Scaling behavior of the spin pumping effect in ferromagnet-platinum bilayers, Phys. Rev. Lett. **107**, 46601 (2011).

[23] M. Weiler, M. Althammer, M. Schreier, J. Lotze, M. Pernpeintner, S. Meyer, H. Huebl, R. Gross, A. Kamra, J. Xiao, Y. T. Chen, H. J. Jiao, G. E. W. Bauer, and S. T. B. Goennenwein, Experimental test of the spin mixing interface conductivity concept, Phys. Rev. Lett. **111**, 176601 (2013).

[24] S. Emori, B. A. Gray, H.-M. Jeon, J. Peoples, M. Schmitt, A. C. Bornstein, P. Shafer, A. T. N. Diaye, E. Arenholz, G. Haugstad, K.-Y. Meng, F. Yang, D. Li, D. G. Cahill, P. Dhagat, A. Jander, N. X. Sun, Y. Suzuki, B. M. Howe, K. Mahalingam, M. Hill, M. E. McConney, M. T. Gray, U. S. Alaan, A. C. Bornstein, P. Shafer, A. T. N'Diaye, E. Arenholz, G. Haugstad, K.-Y. Meng, F. Yang, D. Li, S. Mahat, D. G. Cahill, P. Dhagat, A. Jander, N. X. Sun, Y. Suzuki, and B. M. Howe, Coexistence of Low Damping and Strong Magnetoelastic Coupling in Epitaxial Spinel Ferrite Thin Films, Adv. Mater. **29**, 1701130 (2017).

[25] A. K. Srivastava, M. J. Hurben, M. A. Wittenauer, P. Kabos, C. E. Patton, R. Ramesh, P. C. Dorsey, and D. B. Chrisey, Angle dependence of the ferromagnetic resonance linewidth and two magnon losses in pulsed laser deposited films of yttrium iron garnet, MnZn ferrite, and NiZn ferrite, J. Appl. Phys. **85**, 7838 (1999).

[26] D. Roy, S. Sakshath, G. Singh, R. Joshi, S. V Bhat, and P. S. Anil Kumar, Investigation on two magnon scattering processes in pulsed laser deposited epitaxial nickel zinc ferrite thin film, J. Phys. D. Appl. Phys. **48**, 125004 (2015).

[27] G. Woltersdorf and B. Heinrich, Two-magnon scattering in a self-assembled nanoscale network of misfit dislocations, Phys. Rev. B **69**, 184417 (2004).

[28] O. Mosendz, V. Vlaminck, J. E. Pearson, F. Y. Fradin, G. E. W. Bauer, S. D. Bader, and A. Hoffmann, Detection and quantification of inverse spin Hall effect from spin pumping in permalloy/normal metal bilayers, Phys. Rev. B **82**, 214403 (2010).

[29] C. T. Boone, H. T. Nembach, J. M. Shaw, and T. J. Silva, Spin transport parameters in metallic multilayers determined by ferromagnetic resonance measurements of spin pumping, J. Appl. Phys. **113**, 153906 (2013).

[30] H. L. Wang, C. H. Du, Y. Pu, R. Adur, P. C. Hammel, and F. Y. Yang, Scaling of spin Hall angle in 3d, 4d, and 5d metals from $Y_3Fe_5O_{12}$ /metal spin pumping, Phys. Rev. Lett. **112**, 197201 (2014).

[31] C. Hahn, G. De Loubens, O. Klein, M. Viret, V. V. Naletov, and J. Ben Youssef, Comparative measurements of inverse spin Hall effects and magnetoresistance in YIG/Pt and YIG/Ta, Phys. Rev. B **87**, 174417 (2013).

[32] M. Haertinger, C. H. Back, J. Lotze, M. Weiler, S. Geprägs, H. Huebl, S. T. B. Goennenwein, and G. Woltersdorf, Spin pumping in YIG/Pt bilayers as a function of layer thickness, Phys. Rev. B **92**, 54437 (2015).

[33] M. H. Nguyen, D. C. Ralph, and R. A. Buhrman, Spin torque study of the spin Hall conductivity and spin diffusion length in platinum thin films with varying resistivity, Phys. Rev. Lett. **116**, 126601 (2016).

[34] S. Azzawi, A. Ganguly, M. Tokac, R. M. Rowan-Robinson, J. Sinha, A. T. Hindmarch, A. Barman, and D. Atkinson, Evolution of damping in ferromagnetic/nonmagnetic thin film bilayers as a function of nonmagnetic layer thickness, Phys. Rev. B **93**, 54402 (2016).

[35] J. C. Rojas-Sánchez, N. Reyren, P. Laczkowski, W. Savero, J. P. Attané, C. Deranlot, M. Jamet, J. M. George, L. Vila, and H. Jaffrès, Spin pumping and inverse spin Hall effect in platinum: The essential role of spin-memory loss at metallic interfaces, Phys. Rev. Lett. **112**, 106602 (2014).

[36] C. Burrowes, B. Heinrich, B. Kardasz, E. A. Montoya, E. Girt, Y. Sun, Y. Y. Song, and M. Wu, Enhanced spin pumping at yttrium iron garnet/Au interfaces, Appl. Phys. Lett. **100**, 92403 (2012).

[37] S. Pütter, S. Geprägs, R. Schlitz, M. Althammer, A. Erb, R. Gross, and S. T. B. Goennenwein, Impact of the interface quality of Pt/YIG(111) hybrids on their spin Hall magnetoresistance, Appl. Phys. Lett. **110**, (2017).

[38] A. Azevedo, L. H. Vilela-Leão, R. L. Rodríguez-Suárez, A. F. Lacerda Santos, and S. M. Rezende, Spin pumping and anisotropic magnetoresistance voltages in magnetic bilayers: Theory and experiment, Phys. Rev. B **83**, 144402 (2011).

[39] L. Bai, P. Hyde, Y. S. Gui, C.-M. Hu, V. Vlaminck, J. E. Pearson, S. D. Bader, and A. Hoffmann, Universal method for separating spin pumping from spin rectification voltage of ferromagnetic resonance, Phys. Rev. Lett. **111**, 217602 (2013).

[40] M. Obstbaum, M. Härtinger, H. G. Bauer, T. Meier, F. Swientek, C. H. Back, and G. Woltersdorf, Inverse spin Hall effect in $Ni_{81}Fe_{19}$/normal-metal bilayers, Phys. Rev. B **89**, 60407 (2014).

[41] Y. M. Lu, J. W. Cai, S. Y. Huang, D. Qu, B. F. Miao, and C. L. Chien, Hybrid magnetoresistance in the proximity of a ferromagnet, Phys. Rev. B **87**, 220409 (2013).

[42] D. Qu, S. Y. Huang, B. F. Miao, S. X. Huang, and C. L. Chien, Self-consistent determination of spin Hall angles in selected 5d metals by thermal spin injection, Phys. Rev. B **89**, 140407 (2014).

[43] See Supplemental Material at [URL will be inserted by publisher] for furthur discussion of W coated samples and XMCD results.

[44] T. Tanaka, H. Kontani, M. Naito, T. Naito, D. S. Hirashima, K. Yamada, and J. Inoue, Intrinsic spin Hall effect and orbital Hall effect in 4d and 5d transition metals, Phys. Rev. B **77**, 165117 (2008).

[45] C. F. Pai, L. Liu, Y. Li, H. W. Tseng, D. C. Ralph, and R. A. Buhrman, Spin transfer torque devices

utilizing the giant spin Hall effect of tungsten, Appl. Phys. Lett. **101**, 122404 (2012).

[46] Y. Matsumoto, S. Okamoto, N. Kikuchi, O. Kitakami, Y. Miura, M. Suzuki, M. Mizumaki, and N. Kawamura, Large Negative Magnetic Anisotropy of W/Fe/W (001) Epitaxial Trilayers, IEEE Trans. Magn. **51**, 2100704 (2015).

[47] X. Qian and W. Hübner, Symmetry and substrate effects on magnetic interactions from first principles: A comparison between Fe/W(100) and Fe/W(110), Phys. Rev. B **67**, 184414 (2003).

[48] A. Kashyap, P. Manchanda, P. K. Sahota, R. Skomski, J. E. Shield, and D. J. Sellmyer, Anisotropy of W in Fe and Co, IEEE Trans. Magn. **47**, 3336 (2011).

[49] K. Chen and S. Zhang, Spin pumping induced electric voltage, IEEE Magn. Lett. **6**, 1 (2015).

[50] N. Vliestra, J. Shan, V. Castel, B. J. van Wees, and J. Ben Youssef, Spin-Hall magnetoresistance in platinum on yttrium iron garnet: Dependence on platinum thickness and in-plane / out-of-plane magnetization, Phys. Rev. B **87**, 184421 (2013).

[51] Y.-T. Chen, S. Takahashi, H. Nakayama, M. Althammer, S. T. B. Goennenwein, E. Saitoh, and G. E. W. Bauer, Theory of spin Hall magnetoresistance, Phys. Rev. B **87**, 144411 (2013).

[52] H. Nakayama, M. Althammer, Y. T. Chen, K. Uchida, Y. Kajiwara, D. Kikuchi, T. Ohtani, S. Geprägs, M. Opel, S. Takahashi, R. Gross, G. E. W. Bauer, S. T. B. Goennenwein, and E. Saitoh, Spin Hall Magnetoresistance Induced by a Nonequilibrium Proximity Effect, Phys. Rev. Lett. **110**, 206601 (2013).

[53] M. Althammer, S. Meyer, H. Nakayama, M. Schreier, S. Altmannshofer, M. Weiler, H. Huebl, S. Geprags, M. Opel, R. Gross, D. Meier, C. Klewe, T. Kuschel, J. M. Schmalhorst, G. Reiss, L. Shen, A. Gupta, Y. T. Chen, G. E. W. Bauer, E. Saitoh, and S. T. B. Goennenwein, Quantitative study of the spin Hall magnetoresistance in ferromagnetic insulator/normal metal hybrids, Phys. Rev. B **87**, 224401 (2013).

[54] H. Wang, C. Du, P. C. Hammel, and F. Yang, Comparative determination of $Y_3Fe_5O_{12}$/Pt interfacial spin mixing conductance by spin-Hall magnetoresistance and spin pumping, Appl. Phys. Lett. **110**, 62402 (2017).

[55] M. I. Dyakonov, Magnetoresistance due to edge spin accumulation, Phys. Rev. Lett. **99**, 126601 (2007).

[56] S. Vélez, V. N. Golovach, A. Bedoya-Pinto, M. Isasa, E. Sagasta, M. Abadia, C. Rogero, L. E. Hueso, F. S. Bergeret, and F. Casanova, Hanle Magnetoresistance in Thin Metal Films with Strong Spin-Orbit Coupling, Phys. Rev. Lett. **116**, 16603 (2016).

[57] M. Farle, Ferromagnetic resonance of ultrathin metallic layers, Reports Prog. Phys. **61**, 755 (1998).

[58] H. Wang, C. Du, P. C. Hammel, and F. Yang, Strain-tunable magnetocrystalline anisotropy in epitaxial $Y_3Fe_5O_{12}$ thin films, Phys. Rev. B **89**, 134404 (2014).

[59] S. Vélez, V. N. Golovach, A. Bedoya-Pinto, M. Isasa, E. Sagasta, M. Abadia, C. Rogero, L. E. Hueso, F. S. Bergeret, and F. Casanova, Hanle Magnetoresistance in Thin Metal Films with Strong Spin-

Orbit Coupling, Phys. Rev. Lett. **116**, 16603 (2016).

[60] S. R. Marmion, M. Ali, M. McLaren, D. A. Williams, and B. J. Hickey, Temperature dependence of spin Hall magnetoresistance in thin YIG/Pt films, Phys. Rev. B **89**, 220404 (2014).

[61] M. Suzuki, H. Muraoka, Y. Inaba, H. Miyagawa, N. Kawamura, T. Shimatsu, H. Maruyama, N. Ishimatsu, Y. Isohama, and Y. Sonobe, Depth profile of spin and orbital magnetic moments in a subnanometer Pt film on Co, Phys. Rev. B **72**, 54430 (2005).

[62] M. Valvidares, N. Dix, M. Isasa, K. Ollefs, F. Wilhelm, A. Rogalev, F. Sánchez, E. Pellegrin, A. Bedoya-Pinto, P. Gargiani, L. E. Hueso, F. Casanova, and J. Fontcuberta, Absence of magnetic proximity effects in magnetoresistive Pt/$CoFe_2O_4$ hybrid interfaces, Phys. Rev. B **93**, 214415 (2016).

[63] T. Kuschel, C. Klewe, J. M. Schmalhorst, F. Bertram, O. Kuschel, T. Schemme, J. Wollschläger, S. Francoual, J. Strempfer, A. Gupta, M. Meinert, G. Götz, D. Meier, and G. Reiss, Static Magnetic Proximity Effect in Pt/$NiFe_2O_4$ and Pt/Fe Bilayers Investigated by X-Ray Resonant Magnetic Reflectivity, Phys. Rev. Lett. **115**, 97401 (2015).